

Innovative ultrasound approach to estimate spinal mineral density: diagnostic assessment on overweight and obese women

ISSN 1751-8822

Received on 18th March 2015

Revised on 30th July 2015

Accepted on 19th August 2015

doi: 10.1049/iet-smt.2015.0056

www.ietdl.org

Sergio Casciari¹✉, Paola Pisani¹, Francesco Conversano¹, Maria Daniela Renna¹, Giulia Soloperto², Ernesto Casciari¹, Eugenio Quarta³, Antonella Grimaldi³, Maurizio Muratore³

¹National Research Council, Institute of Clinical Physiology, Lecce, Italy

²Echolight Srl, Lecce, Italy

³O.U. of Rheumatology, Galateo Hospital, San Cesario di Lecce, ASL-LE, Lecce, Italy

✉ E-mail: sergio.casciari@cnr.it

Abstract: The aim of this study is to assess the accuracy of a novel ultrasound (US) approach for lumbar spine densitometry on overweight and obese women of variable age through a clinical validation study. The US method was originally developed in women with body mass index (BMI) < 25 kg/m². In this study, 382 female patients were recruited (45–80 years, BMI > 25 kg/m²) and underwent dual X-ray absorptiometry (DXA) of lumbar spine (L1–L4) and an US scan of the same vertebrae L1–L4, performed with a dedicated device providing both echographic images and ‘raw’ radiofrequency signals. Acquired US data were analysed through a novel automatic algorithm that performed a series of spectral and statistical analyses to calculate bone mineral density employing an innovative method. Diagnostic accuracy of US investigations was quantitatively assessed through a direct comparison with DXA results. The average agreement between US and DXA diagnoses was acceptable for patients aged 45–65 years (81.5%), while a slight decrement was observed for older patients (69.6%), which can be partially due to a decrease in DXA accuracy because of age-related degenerations. The adopted method has a potential for early osteoporosis diagnosis in people younger than 65 years, independent of their BMI.

1 Introduction

Osteoporosis is a chronic skeletal disease that causes reduced bone mass and deterioration of the bone microarchitecture, resulting in an increased risk of fracture [1]. According to the World Health Organization (WHO) diagnostic classification, osteoporosis is identified when bone mineral density (BMD) at the hip or lumbar spine is less than or equal to 2.5 standard deviations (SDs) below the mean value of a young adult reference population [2].

To give an idea of osteoporosis prevalence, we can say that in the Caucasian population ~50% of all women and about 20% of men will experience an osteoporosis-related fracture at some point in their lifetime [2], and these percentages are expected to increase in the next decades because of population ageing.

The most common fractures are those located at spine, hip or wrist [2]. Hip fractures are associated with an excess mortality within 1 year in the range 8–36% [3] and with a 2.5-fold increased risk of future fractures [4]. Vertebral fractures are often associated with disability, deformity and also mortality [5] and, in particular, they are the best predictor of future fracture risk: a vertebral fracture causes an up to five-fold increased risk for a further vertebral fracture and a two- to three-fold increased risk for a different fracture [2].

Unfortunately, osteoporosis still represents an underdiagnosed and undertreated disease [6, 7], essentially because of the lack of a diagnostic tool that is both reliable and suitable for population mass screenings. In fact, the most widely adopted method for osteoporosis diagnosis is dual X-ray absorptiometry (DXA), which is currently considered as the ‘gold standard’ technique for BMD measurements [8–10] and is at the basis of the operational definition of osteoporosis provided by WHO [11]. Actually, DXA has the ability of directly measuring BMD exploiting well-understood physical principles with a good precision and reproducibility [12], which also gave to DXA-based spinal BMD assessments a recognised suitability for therapeutic monitoring

[13]. Nevertheless, the majority of osteoporotic fractures occur in patients having a non-osteoporotic BMD level, indicating that DXA-measured BMD has a low sensitivity in the prediction of fragility fractures, and this is the main reason for which the use of DXA for screening purposes is not generally recommended [14, 15].

As a consequence, osteoporotic fractures currently represent a major cause of public health burden [16]: almost 3 million of new osteoporotic fractures occur yearly in Europe, accounting for a direct cost of about €40 billion and 43,000 related deaths.

Recent studies reported that BMD value, which is routinely employed as a predictor of fracture likelihood [6], is related to different factors, such as body mass index (BMI) and weight, suggesting that BMI should be included in the risk assessment tools for the evaluation of osteoporosis and subsequent probability of fragility fractures [17–20]. In general, overweight is associated with a higher BMD level, although it has to be underlined that this is not always associated with a healthier bone status [21, 22]. Literature-available experimental results support the idea that ultrasound (US) approaches for the evaluation of bone health status can be particularly suitable for diagnostic applications in overweight women [23]. In fact, bone health assessment is just one out of the several biomedical applications of US devices that are being gradually introduced into clinical practice because of their well-known intrinsic advantages over competing technologies (absence of ionising radiation, low costs, portability, availability in primary care settings) [24, 25]. However, the specific clinical routine adoption of US approaches to osteoporosis diagnosis is still hindered by some peculiar aspects, mainly related to the yet incomplete understanding of the physics governing the interaction between bone structures and US waves, which results in indirect BMD measurements, difficulties in standardising methods and devices, and in contradictory opinions about the possible suitability for treatment monitoring purposes. In addition, most of the reported studies of US approaches to bone health assessment were focused on peripheral bone sites (e.g. calcaneus), while the

reference anatomical sites for osteoporosis diagnosis are proximal femur and lumbar spine, and the latter, in particular, has been the less targeted by US investigations [26, 27].

Our research group has recently introduced a new US-based method for vertebral osteoporosis diagnosis based on the comparison between the spectral content of 'raw' backscattered signals and anthropometrically matched spectral models of osteoporotic and healthy vertebrae, previously derived from DXA-diagnosed patients [27]. This novel approach was first tested in normal- and under-weight women aged 51–60 years, providing a very good diagnostic agreement with DXA [27].

In a recent conference paper [28], we preliminarily presented a clinical evaluation of the same approach on a cohort of overweight and obese female patients aged 45–65 years. In the present work, we assessed the performance of the proposed method on a larger study population, also including elderly patients aged 65–80 years. Diagnostic accuracy as a function of patient age and general clinical usefulness of the new approach are critically discussed taking into account the most recent literature. Full details of the adopted protocol for data acquisition and processing are also provided and commented.

2 Materials and methods

2.1 Patients

The study was conducted at the Operative Unit of Rheumatology of 'Galateo' Hospital (San Cesario di Lecce, Lecce, Italy). A total of 382 female patients were enrolled, according to the following criteria: Caucasian ethnicity, aged 45–80 years, BMI > 25 kg/m², absence of significant deambulation impairments, medical prescription for a spinal DXA and signed informed consent.

All the recruited patients underwent two different diagnostic investigations: a conventional spinal DXA and an abdominal US scan of lumbar vertebrae, as detailed in the next paragraphs.

The study protocol was approved by the hospital ethics review board.

2.2 DXA measurements

Spinal DXA scans were performed with hip and knee both at 90° of flexion employing a Discovery W scanner (Hologic, Waltham, MA, USA). BMD was measured over the lumbar tract L1–L4, and the mean value was expressed as grams per square centimetre (g/cm²). For each patient, Hologic software also provided the *T*-score value, defined as the number of SDs from the peak BMD of young women found in the standard Hologic reference database for Caucasian women, and the *Z*-score value, defined as the number of SDs from the mean BMD of age-matched women found in the same standard reference database. According to WHO definitions, patients were classified as 'osteoporotic' if *T*-score ≤ -2.5, 'osteopenic' if -2.5 < *T*-score < -1.0 or 'healthy' if *T*-score ≥ -1.0.

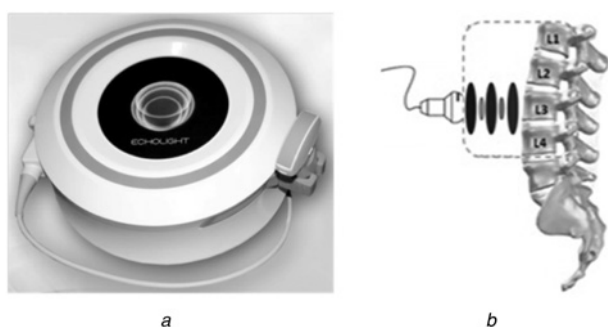


Fig. 1 US acquisition

a Picture of the employed device
b Schematic illustration of the US signal path

2.3 US acquisitions

Abdominal US scans of lumbar vertebrae were performed using an innovative US device developed in Lecce (Italy) within the ECHOLIGHT Project through a collaboration between CNR-IFC (National Research Council – Institute of Clinical Physiology) and Echolight srl. The device was equipped with a 3.5 MHz broadband convex US transducer and configured to provide both echographic images and 'raw' unfiltered radiofrequency (RF) signals, sampled at 40 MS/s. Fig. 1 shows a picture of the employed device and a schematic illustration of the US signal path.

Each patient underwent a sagittal scan of the lumbar vertebrae, by moving the probe back and forth from the xiphoid process. The scan lasted about 1 min and generated 100 frames of RF data (frame-rate ~1.5 fps), which were acquired and stored in a PC hard-disk for subsequent off-line analysis. Transducer focus and scan depth were specifically adjusted for each acquisition in order to have vertebral interfaces located in the US focal region and in the central part of the image. The other acquisition parameters were kept constant to the following values: mechanical index = 0.4, gain = 0 dB and linear time gain compensation.

2.4 US data analysis

Acquired US data were analysed through a novel automatic algorithm that performed a series of spectral and statistical analyses, involving both the echographic images and the underlying RF signals, in order to calculate a new US parameter, called 'osteoporosis score' (O.S.), which has been recently demonstrated to have a strong correlation with BMD in under-weight and normal-weight women [27].

The adopted algorithm performs diagnostic calculations on RF signal segments corresponding to specific regions of interest (ROIs) internal to the vertebrae, which are automatically identified by the algorithm itself (200-point Hamming-windowed signal portions starting after the echo from the vertebral surface, when the amplitude of RF signal envelope reached 15% of its peak value, as shown in Fig. 2). The aim of such calculations is to measure the percentage of vertebral segments whose signal spectral features correlate better with those of an osteoporotic bone model rather than with those of a healthy one. The algorithm actually compares RF spectra calculated from the considered patient dataset with reference models of healthy and osteoporotic vertebrae obtained from previous US acquisitions on DXA-classified patients.

The implementation of the adopted algorithm has been described in detail in a very recent paper [27] and is briefly summarised herein.

The main data analysis steps performed on each patient dataset are:

- (i) Automatic identification of vertebrae within the acquired echographic images.
- (ii) For each vertebra image, automatic identification of a specific RF signal portion for each scan line crossing the bone surface.
- (iii) Classification of each RF signal portion as 'osteoporotic' or 'healthy' on the basis of the correlation between its frequency spectrum and each of the two age-matched models stored in a previously obtained reference database.
- (iv) For each vertebra, calculation of the O.S. value, defined as the percentage of the analysed vertebra segments that were classified as 'osteoporotic' in the previous step.
- (v) Calculation of the O.S. value for the considered patient as the average of the single vertebra values.
- (vi) Calculation of the conventional parameters BMD, *T*-score and *Z*-score, as a function of the O.S. value, through specific equations depending on patient age and BMI.

Fig. 3 shows a typical echographic image frame, both before (Fig. 3a) and after (Fig. 3b) the automatic algorithm processing: Fig. 3b identifies the vertebral surface and the ROI used for RF data analysis, whose coordinates were derived from the iteration,

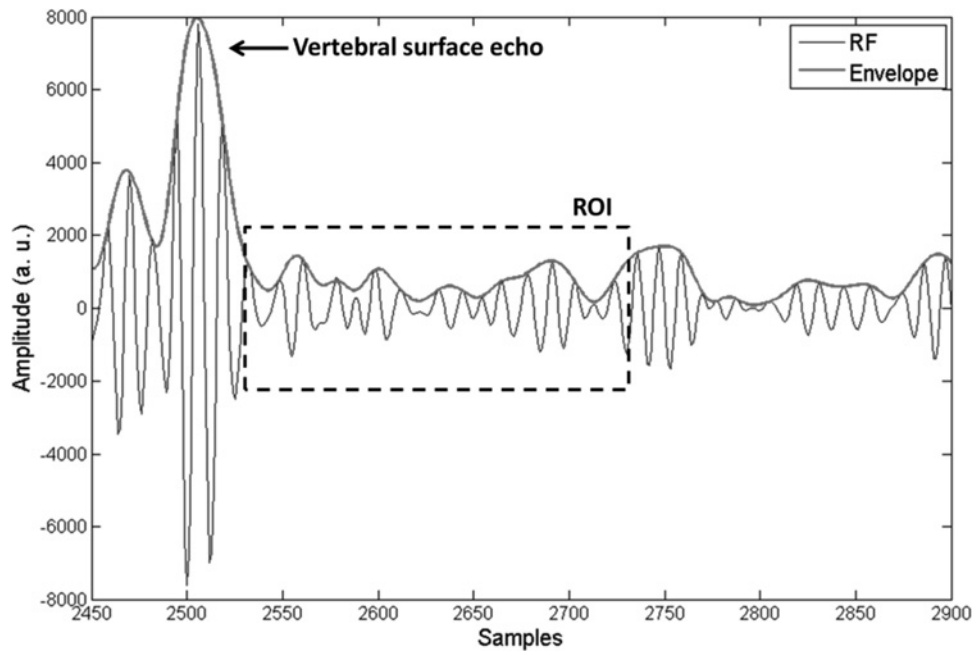


Fig. 2 Identification of the RF signal segment corresponding to the ROI internal to considered vertebra: the selected 200-point RF segment started after the echo from the vertebral surface, when the envelope reached 15% of its peak value. Once identified, the RF segment underwent a simple Hamming windowing and a FFT calculation, in order to obtain the frequency spectrum that was used for the statistical operations described in the text

for all the scan lines crossing the vertebral surface, of the process schematically illustrated in Fig. 2 for a single scan line.

Patients enrolled for the present study were subdivided into seven different age intervals: 45–50 years, 51–55 years, 56–60 years, 61–65 years, 66–70 years, 71–75 years and 76–80 years. For each of these age intervals, a pair of reference spectral models (an ‘osteoporotic’ one and a ‘healthy’ one) was available in a database that had been previously built following the same procedure detailed in [27]. In particular, the subjects used to build the age-matched models had been enrolled through the same inclusion criteria employed in the present study: Caucasian ethnicity, female sex, aged 45–80 years (100 women for each 5-year interval), BMI > 25 kg/m², medical prescription for a spinal DXA investigation. All these patients, after being classified as ‘osteoporotic’, ‘osteopenic’ or ‘healthy’ based on the corresponding DXA outcome and according to WHO definitions, were included in the reference database: for each considered age interval, ‘osteoporotic’ and ‘healthy’ patients were used to build the corresponding models through the procedure described in [27], whereas

‘osteopenic’ patients were used, together with the ‘osteoporotic’ and the ‘healthy’ ones not included in the considered models, in the preliminary assessments of model effectiveness and, once the final models were available, in the derivation of the equations to convert O.S. values in BMD, *T*-score and *Z*-score (see also later in the text).

For a generic patient dataset to be analysed in the present study, once the appropriate spectral models had been identified in the reference database, the first operation performed by the algorithm was the automatic segmentation of the vertebral interfaces within the sequence of acquired images. This was achieved by carrying out the following steps on each considered frame [27] (the block diagram of the adopted algorithm is reported in Fig. 4):

- Rearrangement of image data in a rectangular matrix, in order to simplify the subsequent processing steps (the typical acquired image was composed of 253 scan lines having from 6000 to 10,500 points/line, depending on the scan depth).

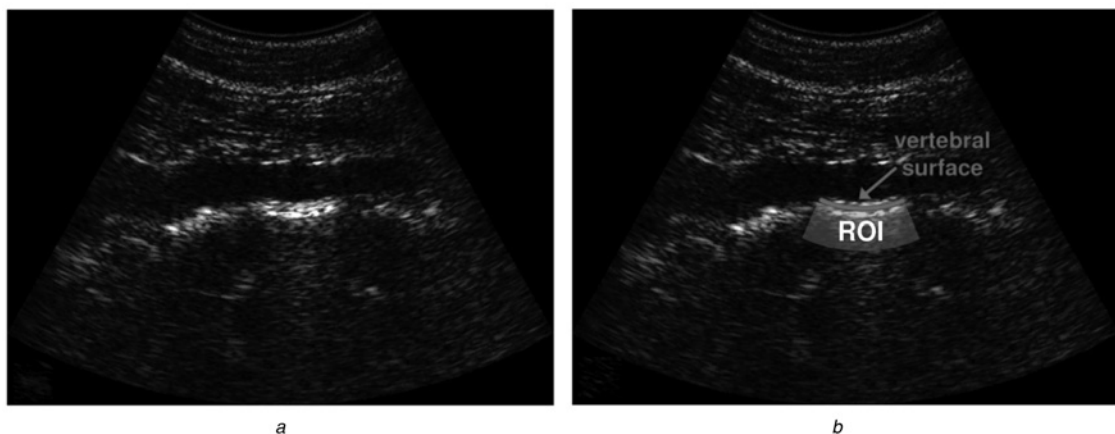


Fig. 3 Typical echographic image frame, which identified both the vertebral surface and the underlying ROI for RF data analysis

a Before the algorithm processing
b After the automatic segmentation

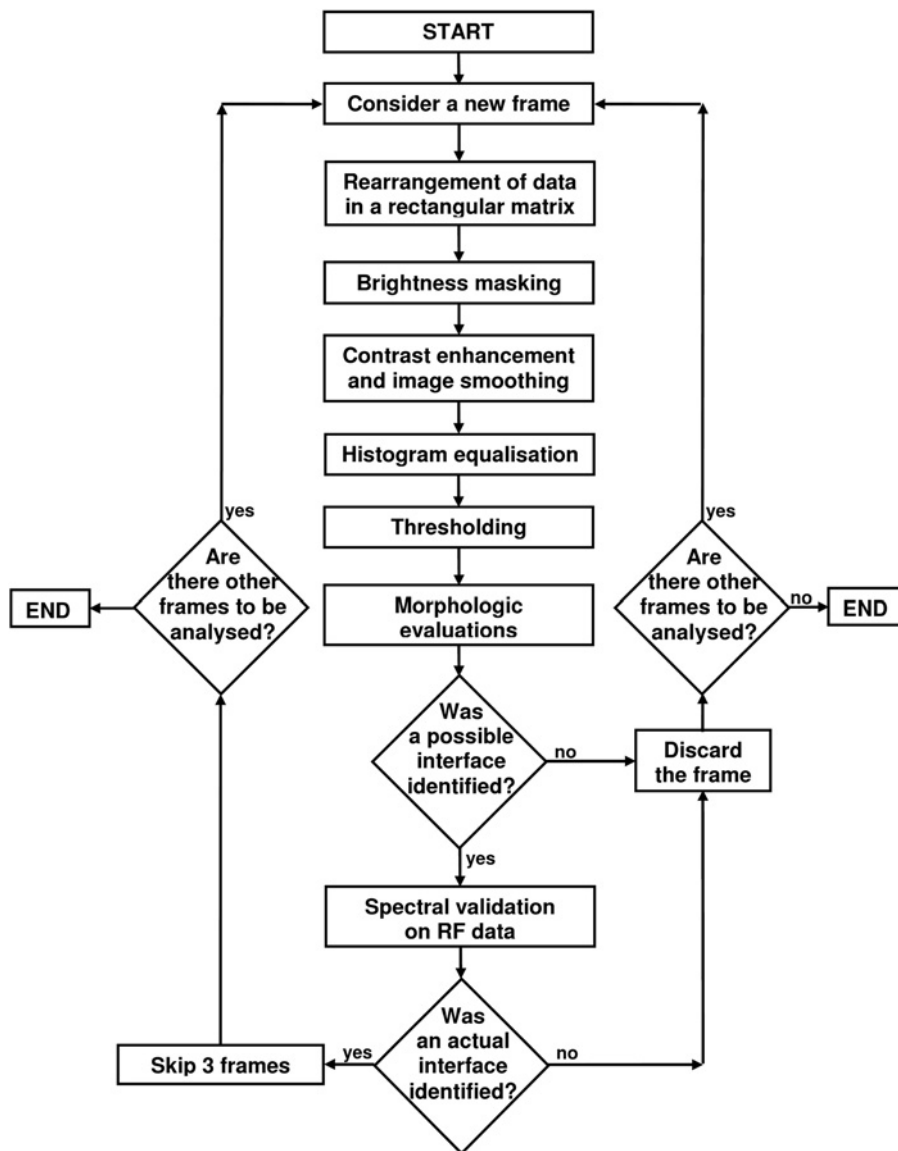


Fig. 4 Block diagram of the algorithm employed for automatic segmentation of the vertebral interfaces within the sequence of acquired images

- Brightness masking, aimed at increasing the brightness of the central region while gradually attenuating brightness level toward image boundaries.
- Contrast enhancement and image smoothing, implemented through the following sequence: (i) pixel values were normalised in the range between '0' and '1'; (ii) contrast-limited adaptive histogram equalisation (the image was divided into 64 identical rectangular regions called 'tiles', each tile's histogram was equalised, and the neighbouring tiles were then combined using a bilinear interpolation, which consists in a linear interpolation performed both horizontally and vertically); (iii) two-dimensional low-pass Gaussian filter (size = 100×100 , SD = 10); (iv) further contrast-limited adaptive histogram equalisation, performed by repeating the same operations done in step ii).
- Histogram equalisation on the entire image (all the histograms involved in this procedure were computed on 256 classes, coinciding with the grey levels of the considered echographic images).
- Thresholding, in order to transform the image into a binary map.
- Morphologic evaluations, aimed at verifying whether, among the white pixel clusters present in the thresholded image, was there a 'possible vertebral interface', which is a cluster of white pixels that has the typical features of a vertebral interface in terms of length, thickness and position. A particularly strict cut-off was based on

measured length: all pixel clusters shorter than 20 mm or longer than 45 mm were filtered out, since their length was outside the typical physiological range for a vertebra height. The clusters whose length was in the expected range were then ranked according to the following criteria: (i) length: two points were assigned to the longest cluster, and one point to the second one; (ii) lateral position: two points were assigned to the cluster that was the best centred in the image along the horizontal direction, and one point to the second one; (iii) vertical position: two points were assigned to the cluster that was the best centred in the image along the vertical direction, and one point to the second one; (iv) average thickness: two points were assigned to the thinnest cluster, and one point to the second one.

- Spectral validation, consisting of a check of the RF data corresponding to the ROI selected below a 'possible vertebral interface' identified in the previous step, in order to verify if the associated spectral content resembled the typical features of a bone structure. This was accomplished by calculating the fast Fourier transform (FFT) spectrum for each RF signal portion belonging to the ROI (Fig. 2) and computing the values of the Pearson correlation coefficient r between the spectrum itself and each of the two appropriate reference model spectra: if at least 70% of the spectra had $r \geq 0.85$ with at least one of the two model spectra the identified interface was labelled as an 'actual vertebral interface'

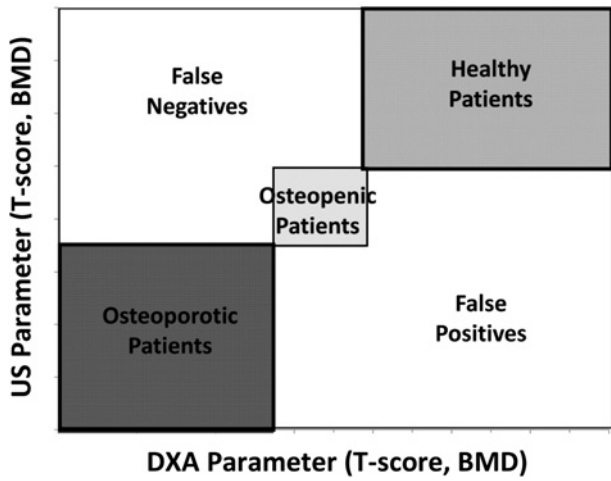


Fig. 5 Scheme of the approach used for the comparison of US and DXA evaluations (in our case, it was possible to classify the patients as osteoporotic, osteopenic or healthy, both by T-score and by BMD since, once the DXA scanner and the investigated anatomical site are fixed, each T-score value is univocally associated to a specific very narrow BMD range)

and the RF data of the corresponding ROI underwent the subsequent analyses (otherwise the frame was discarded). It is important to underline that, if an ‘actual vertebral interface’ was identified in

this step, the subsequent three frames were skipped in order to avoid reconsidering similar views of the same vertebra (otherwise no skip was performed and the subsequent frame was analysed).

Once the listed steps had been performed on all the frames belonging to the analysed patient dataset, the algorithm proceeded to the following diagnostic calculations on the RF signals corresponding to the ROIs selected under the identified vertebral interfaces. The frequency spectrum of each RF signal portion belonging to the considered ROI was classified as ‘osteoporotic’ if the value of its Pearson correlation coefficient with the appropriate osteoporotic model (r_{ost}) was higher than the corresponding correlation value with the related healthy model (r_{heal}), otherwise it was classified as ‘healthy’. Then, the O.S. value for the generic identified vertebra V_i was calculated through the following formula:

$$O.S.V_i = \frac{E_{i_{ost}}}{E_i} \times 100 \quad (1)$$

where $E_{i_{ost}}$ is the number of spectra classified as ‘osteoporotic’ for the vertebra V_i and E_i is the total number of spectra belonging to the ROI.

The O.S. value for the considered patient k is

$$O.S.k = \frac{\sum_{i=1}^{n_k} O.S.V_i}{n_k} \quad (2)$$

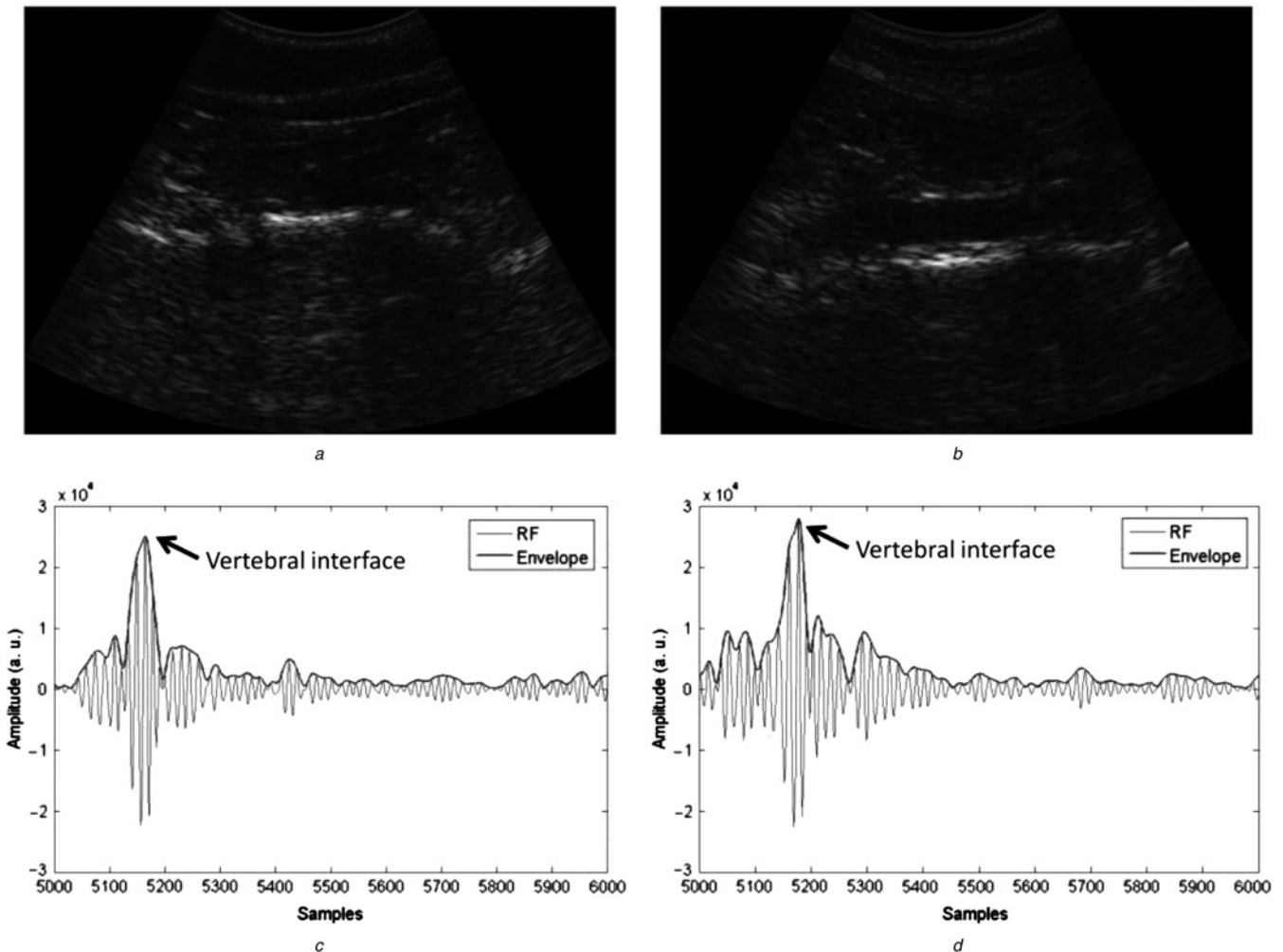


Fig. 6 Typical echographic images and RF signals corresponding to one of the scan lines crossing the vertebral surface

a, c Osteoporotic patient
b, d Healthy patient

where n_k represents the number of vertebrae identified in the dataset corresponding to the patient k .

Finally, the obtained $O.S._k$ value was used as an input parameter to calculate the US-estimated values of BMD, T -score and Z -score through mathematical equations incorporated in the reference model database. For each considered age range, the adopted equations were obtained by employing a linear regression approach to estimate the sought parameter from $O.S.$ values; each equation was derived using the age-matched patients in the reference database, excluding just those used to calculate the models, and was then applied to obtain BMD, T -score and Z -score for the single patients studied in the present work.

Diagnostic accuracy of the obtained results was evaluated through a direct comparison with the corresponding DXA values. Every patient dataset was independently included in a specific diagnostic category (osteoporotic, osteopenic or healthy) by each employed diagnostic technique (i.e. DXA and US): datasets that received the same classification by both the systems were considered as 'correct diagnoses'. A scheme of the approach used for the comparison of US and DXA evaluations is reported in Fig. 5.

Pearson correlation coefficient (r) was also used to assess the correlation between BMD, T -score and Z -score values calculated by the two diagnostic techniques.

3 Results and discussion

Fig. 6 reports a direct comparison between typical echographic images acquired on an osteoporotic patient and on a healthy one, together with the RF signals corresponding to one of the scan lines crossing the vertebral interface. We can note that the two echographic images are qualitatively similar and the same is true for the time-dependent behaviour of single RF signals, with the slight visible differences being due to an occasional coincidence and not to actual characteristics of the two considered diagnostic categories. Therefore, it was not possible to discriminate osteoporotic patients from healthy ones without the described analysis of the spectral content involving a statistically significant number of RF signals. The results obtained through this kind of analysis are illustrated and discussed in the rest of the text.

For 78.3% of the analysed patients US diagnosis (osteoporotic, osteopenic and healthy) coincided with the corresponding DXA one, as visually emphasised by the graphs reported in Figs. 7 and 8.

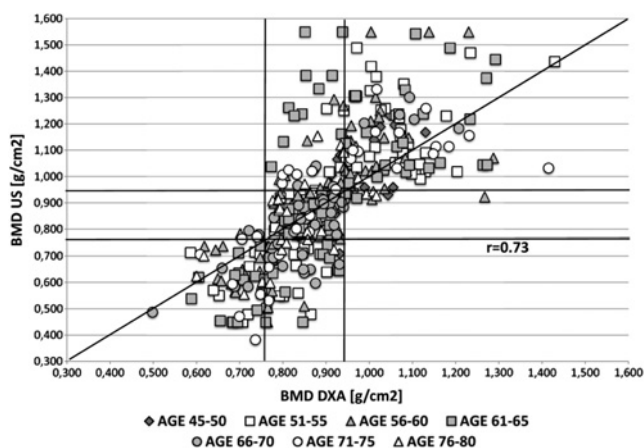


Fig. 7 Scatterplot of US-estimated BMD against the corresponding DXA-measured values for all the considered patient datasets. Line of equality is also shown ($p < 0.001$); the evaluation scheme in Fig. 5 can be used for the identification of correctly diagnosed patients, false positives and false negatives: the horizontal and vertical lines in this graph identify the BMD diagnostic thresholds, which are valid only to classify lumbar spine investigations performed with the DXA scanner model employed in the present study)

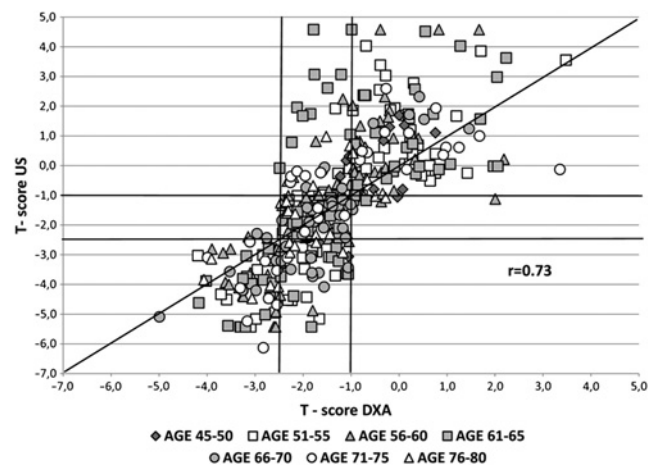


Fig. 8 Scatterplot of T -score values based on US measurements against the corresponding DXA values for all the considered patient datasets. Line of equality is also shown ($p < 0.001$); the evaluation scheme in Fig. 5 can be used for the identification of correctly diagnosed patients, false positives and false negatives: the horizontal and vertical lines in this graph identify the WHO-established T -score diagnostic thresholds)

Fig. 9 shows the corresponding graph obtained for Z -score values. In this case, taking into account the definition of Z -score and the operational definition of osteoporosis, it is not possible the direct identification on the graph of correctly diagnosed patients, false negatives and false positives employing the scheme shown in Fig. 5. However, a statistically significant correlation between US output and corresponding DXA parameter values was found also for Z -score ($r = 0.72$, $p < 0.001$).

Overall, the diagnostic performance of the adopted algorithm, as summarised by the graphs reported in Figs. 7–9 and by the corresponding r values, was only slightly inferior to the one recently reported for the same method applied on thinner women (diagnostic agreement with DXA = 91.1%, $r = 0.84$ [27]), therefore documenting that the proposed approach can be effectively employed for osteoporosis diagnosis independently of patient BMI. In fact, provided that some further tailored optimisations of the adopted method are possible in order to improve the accuracy in the case of overweight and obese patients (as discussed later in the text), the observed differences in diagnostic accuracy with respect to previously reported results [27] can be mainly attributed to the different size of the enrolled study population (382 patients in the present study, 79 in the previous one) and to the wider considered age range (45–80 years versus 51–60 years).

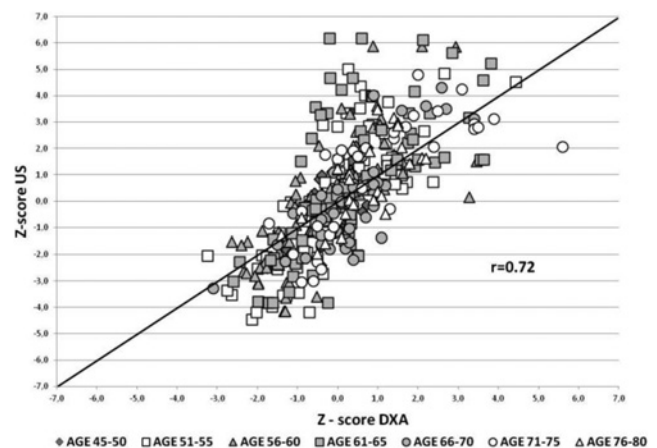


Fig. 9 Scatterplot of Z -score values based on US measurements against the corresponding DXA values for all the considered patient datasets. Line of equality is also shown ($p < 0.001$)

Table 1 Comparison between DXA-measured and US-estimated BMD values as a function of age range

Age range, years	Number of patients	DXA BMD ^a , g/cm ²	US BMD ^a , g/cm ²	Diagnostic agreement, %	Correlation (r)
45–50	22	0.947 ± 0.090	0.968 ± 0.159	86.4	0.76
51–55	75	0.935 ± 0.149	0.959 ± 0.264	81.3	0.76
56–60	98	0.879 ± 0.132	0.897 ± 0.225	83.7	0.74
61–65	85	0.902 ± 0.159	0.929 ± 0.290	77.7	0.66
66–70	44	0.861 ± 0.122	0.834 ± 0.191	63.6	0.79
71–75	32	0.911 ± 0.186	0.910 ± 0.241	78.1	0.73
76–80	26	0.841 ± 0.106	0.849 ± 0.164	65.4	0.67

^amean ± SD.

Actually, the effect of patient age on diagnostic accuracy was studied in detail in the present work and the corresponding results are reported in Table 1. The graphs showing US-estimated BMD against the corresponding DXA-measured values for single age ranges are also reported in Fig. 10 for the most populated age intervals, in order to provide a further visual emphasis on the measured correlation levels as a function of patient age.

From data reported in Table 1, it is evident that the maximum diagnostic accuracy (86.4%) was found in correspondence of the youngest investigated patients (45–50 years), while the minimum accuracy (65.4%) was obtained for the oldest recruited women (76–80 years). Therefore, on one hand, we can say that diagnostic performance of the adopted algorithm was between ‘reasonable’

and ‘good’ for all the studied age intervals, but, on the other hand, a patient age effect on diagnosis accuracy was present and deserved some more detailed comments.

First, it is interesting to observe that the weighted average of diagnostic accuracies for patients in the age interval 45–65 years was 81.5% (range 77.7–86.4%, Table 1), whereas the corresponding weighted average in the age interval 66–80 years was 69.6% (range 65.4–78.1%, Table 1). This is a first indicator that the diagnostic agreement between US and DXA diagnoses is somewhat better for patients younger than 65 years with respect to the older ones.

Second, we can note that diagnostic agreement shows a kind of ‘local peak’ (78.1%, Table 1) in correspondence of the patients aged 71–75 years. Actually, by looking at the average value of DXA BMD for those patients (0.911 ± 0.186 g/cm², Table 1), we can see that this value appears abnormally high with respect to those observed in the other 5-year age intervals regarding patients older than 65 years. In fact, the observed average value of DXA BMD for patients aged 71–75 years is very similar to the corresponding value measured on patients aged 61–65 years (0.902 ± 0.159 g/cm², Table 1). This means that the 32 recruited patients aged 71–75 years, on the average, were healthier than could be expected on the basis of their age, giving a diagnostic agreement between DXA and US diagnoses (78.1%, Table 1) that was very close to the one obtained for patients aged 61–65 years (77.7%, Table 1). Then, taking into account this particular situation for patients aged 71–75 years, the diagnostic agreement for the other patients older than 65 years, whose average values of DXA BMD were aligned with typical expected values, was always

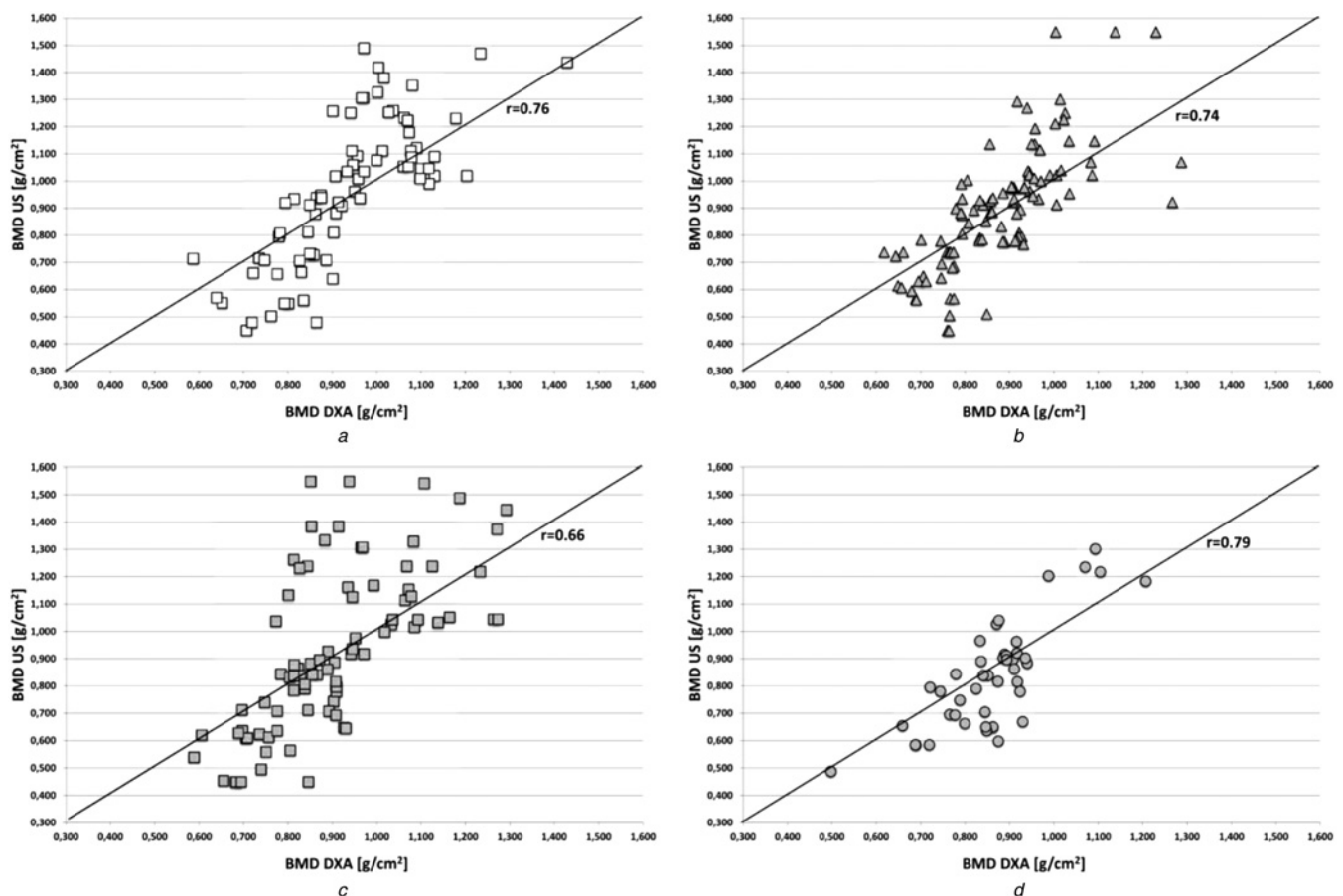


Fig. 10 Scatterplots of US-estimated BMD against the corresponding DXA-measured values for different age ranges

- a 51–55 years
- b 56–60 years
- c 61–65 years
- d 66–70 years

For each reported age range, the line of equality and the calculated value of Pearson correlation coefficient (r) are also shown ($p < 0.001$ for all)

between 65 and 66%. These discrepancies between DXA and US measurements in the elderly patients are not necessarily due to US errors, but they could be at least partially attributed to DXA inaccuracies, since it is known that age-related degenerative changes in the lumbar spine region may affect the accuracy of DXA scans in elderly patients [29–31].

Finally, the values of Pearson correlation coefficient between DXA-measured BMD and corresponding US-obtained results (see Table 1 and Fig. 10) showed a somewhat different trend with respect to the discussed behaviour of diagnostic accuracy (Pearson correlation coefficients referred to *T*-score and *Z*-score measurements were always very close to the *r* values reported in Table 1 and Fig. 10 for BMD measurements). The different trends of diagnostic accuracy and correlation measurements are probably due to the fact that US measurements are intrinsically affected by bone quality properties, which are an important determinant of actual bone strength [32], whereas DXA BMD values directly reflect the calcium content measured in the investigated region. This could in principle represent an added value of the adopted US approach, since it could integrate bone quantity and bone quality providing a final output that is more closely related to the real bone strength, but further dedicated studies are needed to investigate these aspects through detailed comparisons with diagnostic techniques that are intrinsically better suited for bone quality assessment (e.g. quantitative computed tomography [33, 34]).

Overall, independently of bone quality influence, there is at least one possible optimisation of the adopted approach that has the potential to improve the diagnostic agreement with DXA, which reflects the so-called ‘bone quantity’. In fact, the spectral models used in this study had been derived using the same approach described in [27] for thinner women (i.e. they were obtained from patients aged in the same 5-year interval and having BMI in the same range of the considered patient), but while in the case of thin women [27] the condition $BMI < 25 \text{ kg/m}^2$ actually identified a quite narrow BMI range (since patients with $BMI < 20 \text{ kg/m}^2$ are very rare), the actual BMI range identified by the condition $BMI > 25 \text{ kg/m}^2$ was much wider (since, although most of these patients have BMI in the range $25\text{--}30 \text{ kg/m}^2$, a significant portion is distributed in the BMI range $30\text{--}35 \text{ kg/m}^2$ and even beyond). Therefore, the diagnostic accuracy of the proposed approach on overweight and obese women could be further improved, and probably brought to a level similar to the one found for thinner subjects, by specialising the models for narrower BMI ranges. Obviously, this will require a longer recruitment period, in order to ensure a statistically significant number of patients for each BMI range in both reference database and study population.

4 Conclusion

The feasibility of a novel US-based approach for spinal densitometry on overweight and obese women was demonstrated in a wide age interval (45–80 years).

The average diagnostic agreement with reference gold standard represented by DXA was acceptable for patients aged 45–65 years (81.5%), while a slight decrease was observed for older patients (average diagnostic agreement = 69.6%). However, this can be at least partially due to a decrease in DXA accuracy because of age-related degenerations in the lumbar spine region that may affect the reliability of DXA output for elderly patients.

Therefore, on the basis of available results, the adopted method has a potential for early osteoporosis diagnosis through mass population screenings in people younger than 65 years, independently of their BMI. On the other hand, the actual diagnostic accuracy in older patients needs to be verified through further studies employing additional reference techniques (e.g. quantitative computed tomography), which will also quantify the ability of the proposed US methodology to estimate the actual bone strength even better than DXA, thanks to the assessment of bone quality parameters.

5 Acknowledgments

This work was partially funded by FESR P.O. Apulia Region 2007–2013 – Action 1.2.4 (grant no. 3Q5AX31: ECHOLIGHT Project).

6 References

- 1 ‘Prevention and management of osteoporosis’, *World Health Organ. Tech. Rep. Ser.*, 2003, **921**, pp. 1–164
- 2 Cosman, F., de Beur, S.J., LeBoff, M.S., *et al.*: ‘Clinician’s guide to prevention and treatment of osteoporosis’, *Osteoporos. Int.*, 2014, **25**, pp. 2359–2381
- 3 Abrahamsen, B., van Staa, T., Ariely, R., *et al.*: ‘Excess mortality following hip fracture: a systematic epidemiological review’, *Osteoporos. Int.*, 2009, **20**, (10), pp. 1633–1650
- 4 Colón-Emeric, C., Kuchibhatla, M., Pieper, C., *et al.*: ‘The contribution of hip fracture to risk of subsequent fractures: data from two longitudinal studies’, *Osteoporos. Int.*, 2003, **11**, pp. 879–883
- 5 Lewiecki, E.M., Laster, A.J.: ‘Clinical review: clinical applications of vertebral fracture assessment by dual-energy X-ray absorptiometry’, *J. Clin. Endocrinol. Metab.*, 2006, **91**, (11), pp. 4215–4222
- 6 Curtis, J.R., Safford, M.M.: ‘Management of osteoporosis among the elderly with other chronic medical conditions’, *Drugs Aging*, 2012, **29**, pp. 549–564
- 7 van den Bergh, J.P., van Geel, T.A., Geusens, P.P.: ‘Osteoporosis, frailty and fracture: implications for case finding and therapy’, *Nat. Rev. Rheumatol.*, 2012, **8**, pp. 163–172
- 8 Baim, S., Leslie, W.D.: ‘Assessment of fracture risk’, *Curr. Osteoporos. Rep.*, 2012, **10**, pp. 28–41
- 9 Link, T.M.: ‘Osteoporosis imaging: state of the art and advanced imaging’, *Radiology*, 2012, **263**, pp. 3–17
- 10 Schnitzer, T.J., Wysocki, N., Barkema, D., *et al.*: ‘Calcaneal quantitative ultrasound compared with hip and femoral neck dual-energy X-ray absorptiometry in people with a spinal cord injury’, *PM R*, 2012, **4**, pp. 748–755
- 11 Kanis, J., McCloskey, E.V., Johansson, H., *et al.*: ‘A reference standard for the description of osteoporosis’, *Bone*, 2008, **42**, pp. 467–475
- 12 El Maghraoui, A., Roux, C.: ‘DXA scanning in clinical practice’, *Q. J. Med.*, 2008, **101**, pp. 605–617
- 13 Lewiecki, E.M.: ‘Bone densitometry and vertebral fracture assessment’, *Curr. Osteoporos. Rep.*, 2010, **8**, pp. 123–130
- 14 ‘Assessment of fracture risk and its application to screening for postmenopausal osteoporosis’, *World Health Organ. Tech. Rep. Ser.*, 1994, **843**, pp. 1–129
- 15 Kanis, J.A., on behalf of the World Health Organization Scientific Group: ‘Assessment of osteoporosis at the primary health-care level’. Technical Report, World Health Organization Collaborating Centre for Metabolic Bone Diseases, University of Sheffield, UK, 2007
- 16 Cummings, S.R., Melton, L.J.: ‘Epidemiology and outcomes of osteoporotic fractures’, *Lancet*, 2002, **359**, (9319), pp. 1761–1767
- 17 Beranger, G.E., Pisani, D.F., Castel, J., *et al.*: ‘Oxytocin reverses ovariectomy-induced osteopenia and body fat gain’, *Endocrinology*, 2014, **155**, (4), pp. 1340–1352
- 18 Salamat, M.R., Salamat, A.H., Abedi, I., *et al.*: ‘Relationship between weight, body mass index, and bone mineral density in men referred for dual-energy X-ray absorptiometry scan in Isfahan, Iran’, *J. Osteoporos.*, 2013, **2013**, pp. 1–7, id: 205963
- 19 Szklarska, A., Lipowicz, A.: ‘BMI, hypertension and low bone mineral density in adult men and women’, *Homo*, 2012, **63**, (4), pp. 282–291
- 20 De Laet, C., Kanis, J.A., Oden, A., *et al.*: ‘Body mass index as a predictor of fracture risk: a metaanalysis’, *Osteoporos. Int.*, 2005, **16**, (11), pp. 1330–1338
- 21 Sarkis, K.S., Pinheiro Mde, M., Szejnfeld, V.L., *et al.*: ‘High bone density and bone health’, *Endocrinología y Nutrición*, 2012, **59**, (3), pp. 207–214
- 22 Marwaha, R.K., Tandon, N., Gupta, Y., *et al.*: ‘The prevalence of and risk factors for radiographic vertebral fractures in older Indian women and men: Delhi vertebral osteoporosis study (DeVOS)’, *Arch. Osteoporos.*, 2012, **7**, (1–2), pp. 201–207
- 23 Steinschneider, M., Hagag, P., Rapoport, M.J., *et al.*: ‘Discordant effect of body mass index on bone mineral density and speed of sound’, *BMC Musculoskelet. Disord.*, 2003, **4**, (15), pp. 1–6
- 24 Casciaro, S., Conversano, F., Casciaro, E., *et al.*: ‘Automatic evaluation of progression angle and fetal head station through intrapartum echographic monitoring’, *Comput. Math. Methods Med.*, 2013, (2013), pp. 1–8
- 25 Soloperto, G., Conversano, F., Greco, A., *et al.*: ‘Advanced spectral analyses for real time automatic echographic tissue-typing of simulated tumour masses at different compression stages’, *IEEE Trans. Ultrason. Ferroelectr. Freq. Control*, 2012, **59**, (12), pp. 2692–2701
- 26 Garra, B.S., Locker, M., Felker, S., *et al.*: ‘Measurements of ultrasonic backscattered spectral centroid shift from spine in vivo: methodology and preliminary results’, *Ultrasound Med. Biol.*, 2009, **35**, pp. 165–168
- 27 Conversano, F., Franchini, R., Greco, A., *et al.*: ‘A novel ultrasound methodology for estimating spine mineral density’, *Ultrasound Med. Biol.*, 2015, **41**, (1), pp. 281–300
- 28 Casciaro, S., Renna, M.D., Conversano, F., *et al.*: ‘Clinical evaluation of a novel ultrasound-based methodology for osteoporosis diagnosis on overweight and obese women’. Proc. of 3rd Imeko TC13 Symp. on Measurements in Biology and Medicine. ‘New Frontiers in Biomedical Measurements’, Lecce, Italy, April 2014, pp. 45–49
- 29 Chanchairujira, K., Chung, C.B., Kim, J.Y., *et al.*: ‘Intervertebral disk calcification of the spine in an elderly population: radiographic prevalence, location, and

- distribution and correlation with spinal degeneration', *Radiology*, 2004, **230**, pp. 499–503
- 30 Engelke, K., Gluer, C.-C.: 'Quality and performance measures in bone densitometry. Part 1: errors and diagnosis', *Osteoporos. Int.*, 2006, **17**, pp. 1283–1292
- 31 Rand, T., Seidl, G., Kainberger, F., *et al.*: 'Impact of spinal degenerative changes on the evaluation of bone mineral density with dual energy X-ray absorptiometry (DXA)', *Calcif. Tissue Int.*, 1997, **60**, pp. 430–433
- 32 Raum, K., Grimal, Q., Varga, P., *et al.*: 'Ultrasound to assess bone quality', *Curr. Osteoporos. Rep.*, 2014, **12**, (2), pp. 154–162
- 33 Burghardt, A.J., Pinalat, J.B., Kazakia, G.J., *et al.*: 'Multicenter precision of cortical and trabecular bone quality measures assessed by high-resolution peripheral quantitative computed tomography', *J. Bone Miner. Res.*, 2013, **28**, pp. 524–536
- 34 MacNeil, J.A., Boyd, S.K.: 'Improved reproducibility of high-resolution peripheral quantitative computed tomography for measurement of bone quality', *Med. Eng. Phys.*, 2008, **30**, pp. 792–799